Relation between composition, microstructure and oxidation in iron aluminides

M. Martinez, B. Viguier, P. Maugis and J. Lacaze

CIRIMAT, UMR 5085, ENSIACET, 31077 Toulouse Cedex 4, France

Abstract

The relation between chemical composition, microstructure and oxidation properties has been investigated on various FeAl based alloys, the aim being to induce changes in the microstructure of the compound by selective oxidation of aluminium. Oxidation kinetics that was evaluated on bulk specimens showed that, due to fast diffusion in the alloys, no composition gradient is formed during the aluminium selective oxidation. Accordingly, significant aluminium depletion in the compound could be observed in the thinnest part of oxidised wedge-shape specimens. Another way to obtain samples of variable aluminium content was to prepare diffusion couples with one aluminide and pure iron as end members. These latter specimens have been characterised using electron microscopy and first results of oxidation experiments are presented.

Keywords: A. Iron aluminides, based on FeAl; B. Diffusion; B. Order/disorder transformations; B. Oxidation

1. Introduction

Iron aluminides (Fe–Al alloys with about 20–50 at.% Al) are one among the most widely studied intermetallic compounds due to their good oxidation resistance, their low density with respect to steels and their relatively low costs. Low room temperature ductility has been a major impediment for mechanical processing of these materials, while a drop in strength above 600 °C limits their applications [1]. Recent research indicates that doping and microstructure control can improve the mechanical properties of this class of alloys [2], [3] and [4].

Iron aluminides exhibit order–disorder transformations and large concentrations of defects that depend on temperature and composition [5] and [6]. In the Fe-rich portion of the Fe–Al binary diagram exist the disordered A2 and the ordered B2 (FeAl) and $D0_3$ (Fe_3Al) phases [7], as shown in Fig. 1a. It is accepted since long that the ordering transformations begin with the formation of small ordered nuclei, which eventually grow until they occupy the entire volume of the crystal, resulting in an anti-phase domain structure that is usually characterised by transmission electron microscopy [8]. Different types of anti-phase boundaries are present in the ordered alloys depending on their structure. In B2 ordered alloys only one type of anti-phase boundary is found, the B2-type APB (or APB1) that is formed through the A2 → B2 ordering transformation and that has a fault vector $a/2\langle 111\rangle$ (where a is the lattice parameter of the B2 unit cell). In ordered $D0_3$ two types of anti-phase boundaries can appear: the APB1 that forms as above, with a fault vector $a_0/4\langle 111\rangle$ (where a_0 is the lattice parameter of the $D0_3$ unit cell) and the $D0_3$-type APB (or APB2) related to the B2 → $D0_3$ transformation with a fault vector $a_0/2\langle 100\rangle$ [9], [10], [11] and [12]. The unit cells and the fault vectors are shown in Fig. 1b.

Fig. 1. (a) Fe–Al binary phase diagram [7]; (b) unit cells of the ordered B2 and $D0_3$ phases showing displacement vectors corresponding to APB1 (in B2 cell) and APB2 (in $D0_3$ cell).

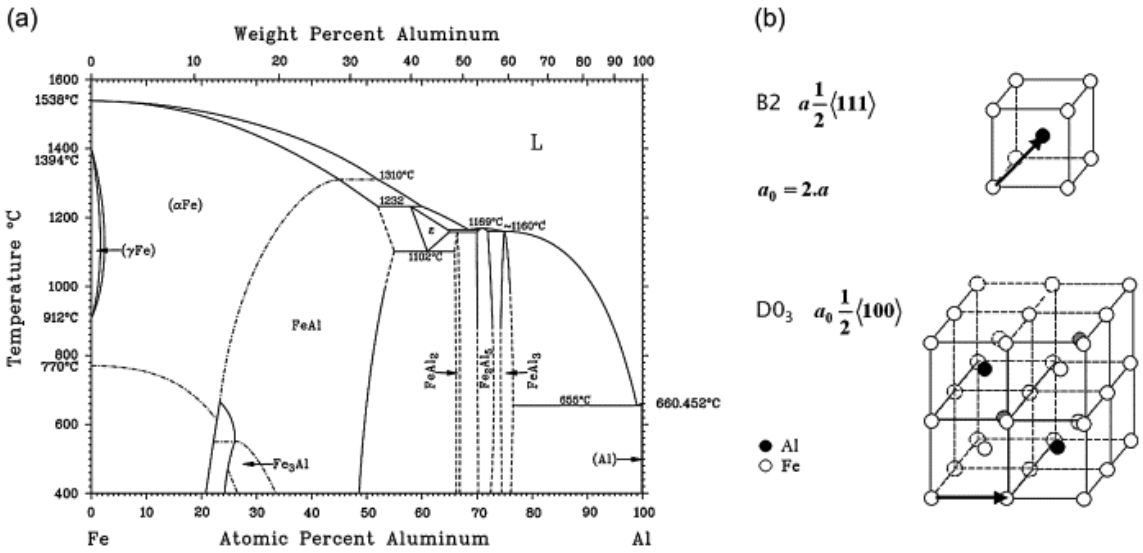

The objective of the present work is to study the relation between composition, microstructure and oxidation, and more particularly the influence of oxidation on the defect structure and phase constitution of iron aluminides, including possible changes in the domain structure. Selective oxidation of aluminium leads to a flux of this species to form the scale and may imply a vacancy injection into the metal. Furthermore, the decrease in the aluminium content of the material may lead to an order–disorder transformation. The final aim of the present study is thus to determine how changes of composition and vacancy injection affect the defect structure of iron aluminides. On the other hand, differences in the alloy composition will induce different microstructures and thus may change the oxidation behaviour.

We present in this paper results obtained on different types of specimens. Thick specimens were used for studying the oxidation kinetics by thermogravimetry. From these data, we show that it is necessary to oxidise thin specimens in order to get significant aluminium depletion, and this prediction led to prepare and test wedge-shape specimens. Finally, we describe how we prepared and characterised specimens with variable composition and microstructure using diffusion couples.

2. Experimental

The chemical compositions of the alloys used in this work are listed in Table 1. The three model alloys, labelled FA, FAB and FANB, were provided by the School of Mines in Saint-Etienne (France), whilst the industrial one labelled FAY is grade 3 alloy developed by CEA (Grenoble, France). These alloys have been studied previously [13] and [14]. Samples of

$10 \times 10 \times 1$ mm^3 were cut out from the provided materials and used for the first oxidation experiments for evaluation of oxidation kinetics. As described later in the text, it appeared necessary to have smaller thickness to ensure enough aluminium depletion in the alloy. Then samples of FANB with variable thickness, from 10 to 200 μm, were prepared and oxidised. To elaborate these kinds of samples we first obtained a slice of constant thickness (200 μm) by grinding, which was then mounted in a wedged support and thinned by one side to around 10 μm while the other side remained at the initial thickness. Finally, in order to study the role of composition on microstructure and on the oxidation behaviour, we prepared samples with variable composition that were obtained from diffusion couples. These diffusion couples were prepared by clamping together iron aluminide pieces and iron. Parallelepipeds of about $5 \times 5 \times 5$ mm^3 in size were cut out from the four iron aluminides while the iron used was a foil of 1.5 mm in thickness. The purity of iron was 99.95%, the remaining being essentially carbon. One flat surface of each sample was prepared metallographically, i.e. polished down to 3 μm diamond paste. The diffusion couples were then assembled in a sample holder and heat treated for 168 h at 1000 °C in a resistance furnace under an argon flux. The diffusion couples were finally furnace cooled. The microstructure of the diffusion couples was revealed by means of two chemical etchants: a mixture of 18% HNO_3, 10% HCl, 5% $C_2H_4O_2$, 1% HF and 66% H_2O to reveal the grains and nital (4%) to contrast cementite precipitates and pearlite. Oxidation of the diffusion couples was carried out on samples 1 mm thickness cut off along the diffusion path.

Table 1.

Chemical composition (at.%) of the different alloys that were used in this study, together with the label by which the alloys are designated in the text [13] and [14]

Alloy	**Label**	**Fe**	**Al**	**Ni**	**Y**	**B**
Fe–Al	FA	Bal.	38.8	–	–	–
Fe–Al–B	FAB	Bal.	39.6	–	–	0.02
Fe–Al–Ni–B	FANB	Bal.	40.2	3.8	–	0.04
Fe–Al–Y_2O_3	FAY	Bal.	39.2	–	1.0	–

All the isothermal oxidation treatments were performed in a SETARAM TAG24 thermal analyzer at 800 °C in synthetic air, with a flow rate of about 1.2 l/h with an accuracy of 1 μg.

Before testing, the samples were polished with 600 grit emery paper and then cleaned with acetone and ethanol.

Observation of the surface of the oxidised samples was achieved by scanning electron microscopy (SEM) performed on a LEO 535 VP microscope operating at 15 kV. Chemical analyses were performed in the SEM using an energy dispersive spectroscopy (EDS) system by PGT. Comparison of EDS measurements on bulk samples with chemical analysis showed that the former lead to a systematic overestimation of the aluminium content which amounts to about 2.5 at.% at 40 at.% Al. Such a bias is supposed to be due to the calibration of the EDS system. To estimate the scale thickness, a section perpendicular to the oxidised surface was then cut out from the sample and prepared by first sputtering with silver, then depositing a layer of nickel and finally mounting in resin for metallographic preparation. Microstructural observation of the phases and characterisation of the domain structure was made by transmission electron microscopy (TEM) with a JEOL 2010 (TEMSCAN service of University Paul Sabatier, Toulouse, France) operating at 200 kV. Some of the thin foils were prepared by the twin jet method, with an electrolyte consisting of 30% of nitric acid and 70% of methanol; others were obtained by ion bombardment of argon in a precision ion polishing system from Gatan.

3. Results and discussion

3.1. Samples of constant and variable thickness

It has been previously shown [15] that the oxidation kinetics of FANB alloy is slow and that the scale is composed of a mixture of aluminium oxides (α-Al_2O_3 + θ-Al_2O_3). Similar observations were made for the other alloys, in particular for what concerns the parabolic rate constants for oxidation, denoted k_p, which are given in Table 2. As a matter of fact, the values in Table 2 are by far much lower than the value of 1×10^{-2} mg^2 cm^{-4} s^{-1} reported for iron oxides [16]. Such low k_p values suggest that the oxide which is formed is composed of alumina and no iron oxides were formed. In other words, the aluminium content in these alloys is high enough to ensure the production of an oxide layer composed only of alumina, which is a slow-growing phase. From Table 2, it is seen that the FAY alloy has a much lower oxidation kinetics than FAB, and that the addition of Ni to this latter alloy improves significantly its oxidation resistance (oxidation kinetics of FA alloy has not yet been evaluated).

Table 2.

Parabolic oxidation rate constants k_p determined during isothermal oxidation at 800 °C in synthetic air

Label	k_p **(mg^2 cm^{-4} s^{-1})**
FAB	7.36×10^{-8}
FANB	2.76×10^{-8}
FAY	9.85×10^{-9}

During oxidation, the diffusion flux of aluminium is driven by oxidation kinetics. In the case where the aluminium reservoir is large enough (thick specimen) so that the bulk composition remains constant at its initial value (X_0), a flux balance at the oxide/metal interface and the diffusion laws allow calculating the composition profile in the alloy and the composition at the scale/metal interface (X_S). Considering an average and composition independent inter-diffusion coefficient (D), one has:

$$X_S = X_0 - \frac{V_m}{3M_O}\sqrt{\frac{\pi k_p}{D}} \quad (1)$$

where V_m is the molar volume of FeAl and M_O the molar mass of oxygen. From the above considerations, one may expect a diffusion profile as schematically illustrated in Fig. 2 when the ratio k_p/D is high enough. In such a case, the diffusion profile intersects the composition X_T at which the material disorders through the transformation B2 → A2. In the present case however, the oxidation of the alloy is slow compared to the diffusion of aluminium in FeAl [17] and [18] so that k_p/D is low and $X_S \sim X_0$. Indeed, due to the relatively fast diffusion, the composition under the oxide scale is continuously homogenised and the whole thickness of the sample serves as an aluminium reservoir. Consequently, the composition profile is almost flat and very long oxidation times would be necessary to achieve significant aluminium depletion in the iron aluminide.

Fig. 2. Schematic drawing of a composition profile that may be produced in a FeAl compound by selective oxidation of aluminium with a high k_p/D ratio (see text).

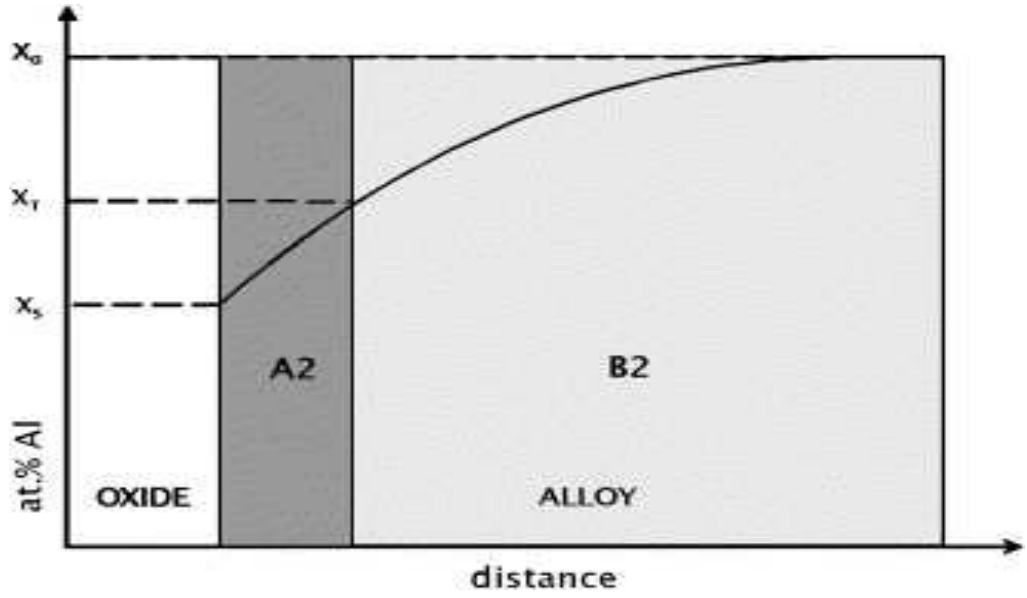

Thin samples of variable thickness were thus prepared because they have a smaller aluminium reservoir, and then oxidised. The relationship between the aluminium content after the oxidation test and the thickness of the sample is illustrated in Fig. 3 in the case of alloy FANB. The shadowed area represents the variation of the specimen thickness with the position *y* along the length of the sample. Assuming that there is no diffusion of aluminium in the *y* direction, the composition $X(y)$ is then obtained through a mass balance considering the relationship between the supply and consumption of aluminium. This gives:

$$X(y) = X_0 - \frac{4V_m}{3M_O}\frac{\sqrt{k_p t}}{e(y)} \qquad (2)$$

where $e(y)$ is the thickness of the sample at *y* and *t* is time. The result of the calculation based on Eq. (2) is shown in Fig. 3 together with the experimental composition profile as measured by EDS in the SEM. These results show that the depletion in aluminium becomes important for thicknesses of 50 μm and less, which confirms that very thin samples should be oxidised in order to promote the B2 → A2 transformation. In the present case, the transition has not taken place and the sample will be prepared for TEM observations to investigate the possible effect of vacancy injection on the defect structure of the B2 phase.

Fig. 3. Aluminium concentration profile of the FANB sample of variable thickness versus the position, as measured experimentally by EDS in the SEM (♦) and calculated using Eq. (2) (—

). The corresponding thickness is indicated by the shadowed area. The sample was oxidised at 800 °C for 100 h in synthetic air.

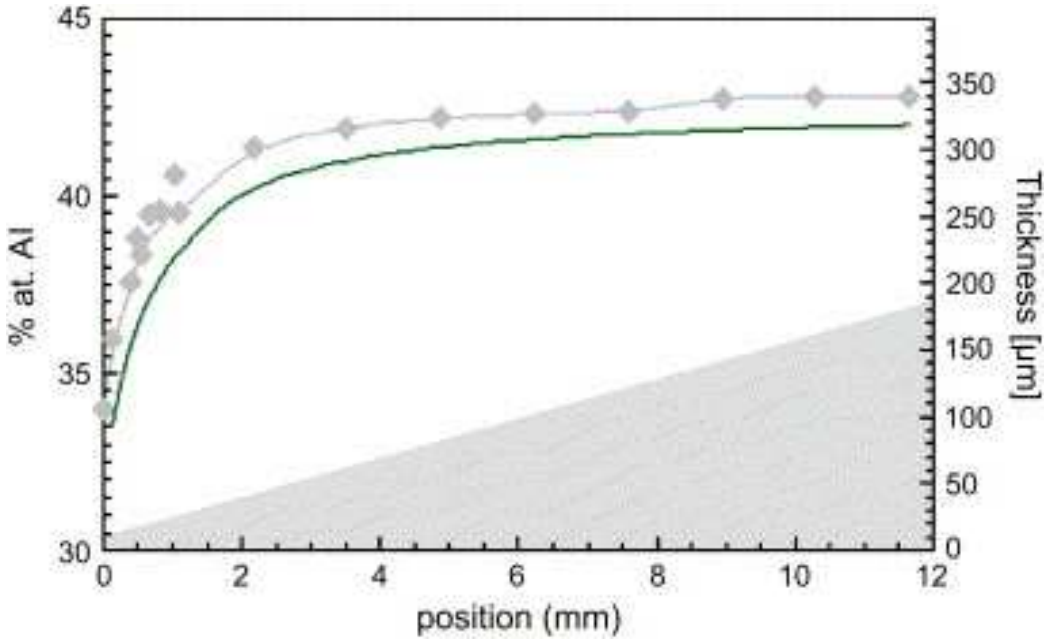

3.2. Samples of variable composition

After the preparation process and the heat treatment described in Section 2, a section along the diffusion path of each diffusion couple was cut out and prepared for metallographic observations. All four diffusion couples presented the same features that are illustrated in Fig. 4a where the section obtained in the case of the FA alloy with the aluminium profile superimposed is shown. The origin of the axis along the length of the diffusion profile corresponds to the initial junction of the diffusion couple, with pure iron above and the iron aluminide below. Three microstructural zones are evidenced as described below.

Fig. 4. The microstructure revealed by chemical etching of the diffusion couple obtained between FA alloy and iron is shown in (a) with the aluminium concentration profile superimposed. The corresponding phase fields are given at 1000 °C (b) and 400 °C (c). The horizontal line indicates the original contact surface of the couple.

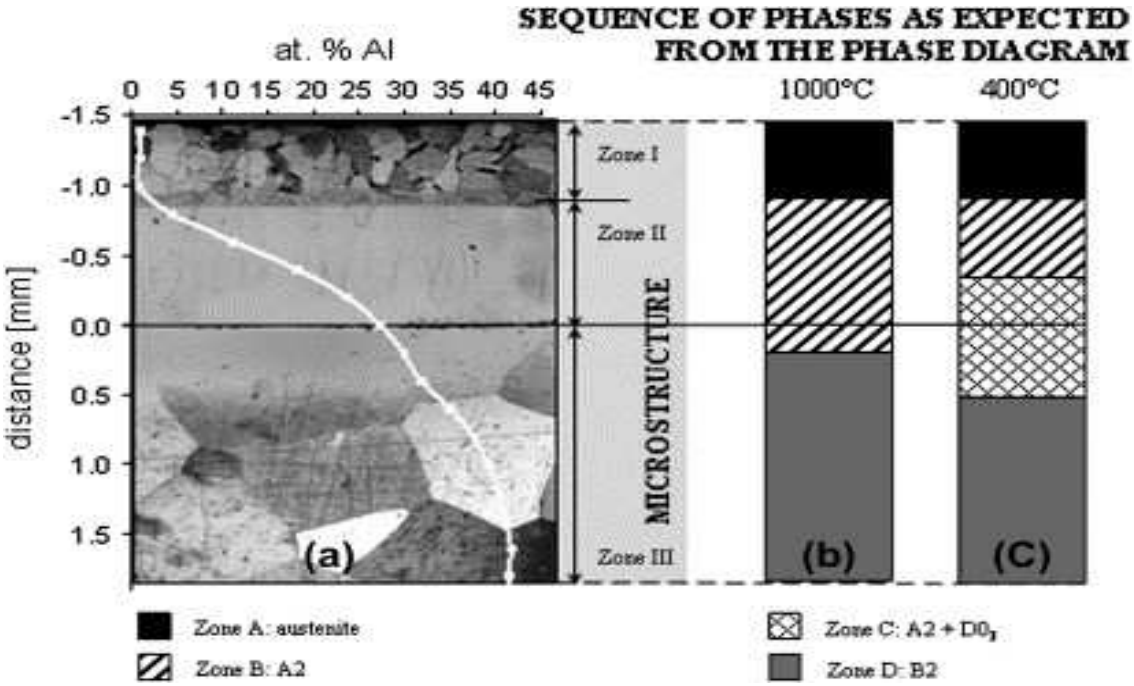

Zone I consists of large grains (about 100 μm) and some limited areas in dark contrast. The aluminium content is low, so that these grains are iron which was present as austenite at the heat-treatment temperature. During cooling, at the end of the heat treatment, austenite transformed into ferrite and pearlite, the latter corresponding to the zones in dark contrast.

Zone II is defined as the zone between zone I and the initial junction. It is composed of elongated grains and has an aluminium content between 4 and 27 at.% and thus consisted of A2 phase at the heat treatment temperature. The disordered A2 phase first formed at the junction of the diffusion couple and grew at the expense of the austenite. This directional growth process leads to the columnar structure in zone II. As the A2 phase has a very low solubility for carbon, this species was rejected in the remaining austenite in zone I.

Zone III that is composed of very large grains similar to that of the initial FA alloy. In this zone, the aluminium content varies between 27 and 41 at.%. According to the phase diagram in Fig. 1a, this zone should consist of disordered A2 phase between 27 and 30 at.% Al and of the ordered B2 phase for higher aluminium content.

In Fig. 4b, three zones labelled A, B and D show the three different domains in terms of phases present at the heat-treatment temperature. These are austenite (zone A), A2 (zone B) and B2 (zone D). During the cooling of the diffusion couple after the heat treatment partial transformation of A2 or B2 into ordered $D0_3$ phase took place. Taking as an example the

phase boundaries at 400 °C given in Fig. 1a, $D0_3$ could be present for aluminium contents in between 20 and 35 at.%. This is illustrated in Fig. 4c which shows a fourth zone, labelled C, appearing in between zones B and D in Fig. 4b and corresponding to the presence of $D0_3$.

Fig. 5 presents TEM images made around the [110] zone axis corresponding to locations selected at increasing aluminium contents in the case of the couple with FA alloy. The anti-phase boundaries were imaged using the superlattice reflection $(111)_{D03}$ as shown in Fig. 5b–d. The APB2 domains appear swirling and isotropically oriented. At lower aluminium contents (around 20 at.% Al) the image shows the precipitation of ordered $D0_3$ particles in a matrix rather than an authentic domain structure (Fig. 5a). The relation between the average domain size (measured by line intercepts) and the aluminium content is shown in Fig. 5e, where it is seen that the average size increases with the aluminium content. The domain size obtained in these diffusion couples at about 25 at.% Al (Fig. 5b) is much smaller when compared with that observed in a Fe_3Al alloy cooled at 3.6 °C/h [8].

Fig. 5. Transmission electron microscopy images around the [110] zone axis of the diffusion couple between FA alloy and iron. The images correspond to a series of locations along the diffusion path with increasing Al contents: (a) 20 at.%; (b) 25 at.%; (c) 27 at.% and (d) 30 at.%. (e) Evolution of the domain size with the local composition.

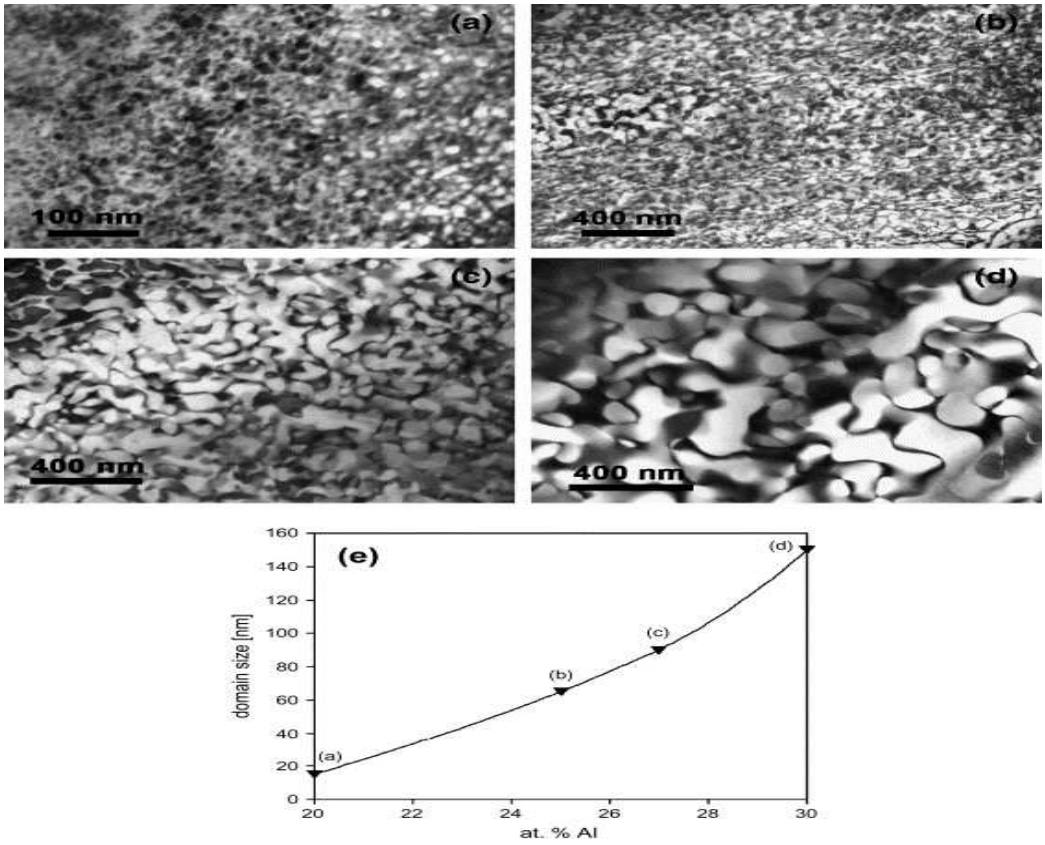

The concentration profiles along two diffusion couples, iron-FA and iron-FAB, are shown in Fig. 6, where the origin of the abscissa corresponds as before to the initial contact surface between iron and iron aluminide. A diffusion profile calculated by a finite difference method and using the diffusion data of Nishida et al. [18] has been superimposed. According to this author, the inter-diffusion coefficient *D* depends on the aluminium concentration and exhibits a sharp maximum at the order–disorder phase transition. The calculation thus shows that the reduction of the slope observed on the experimental diffusion profiles in Fig. 6, at about 30 at.% Al, relates to the maximum of *D*.

Fig. 6. Comparison of experimental diffusion profiles for the couples with FA (■) and FAB (♦) alloys with the profile calculated by a finite difference method (—).

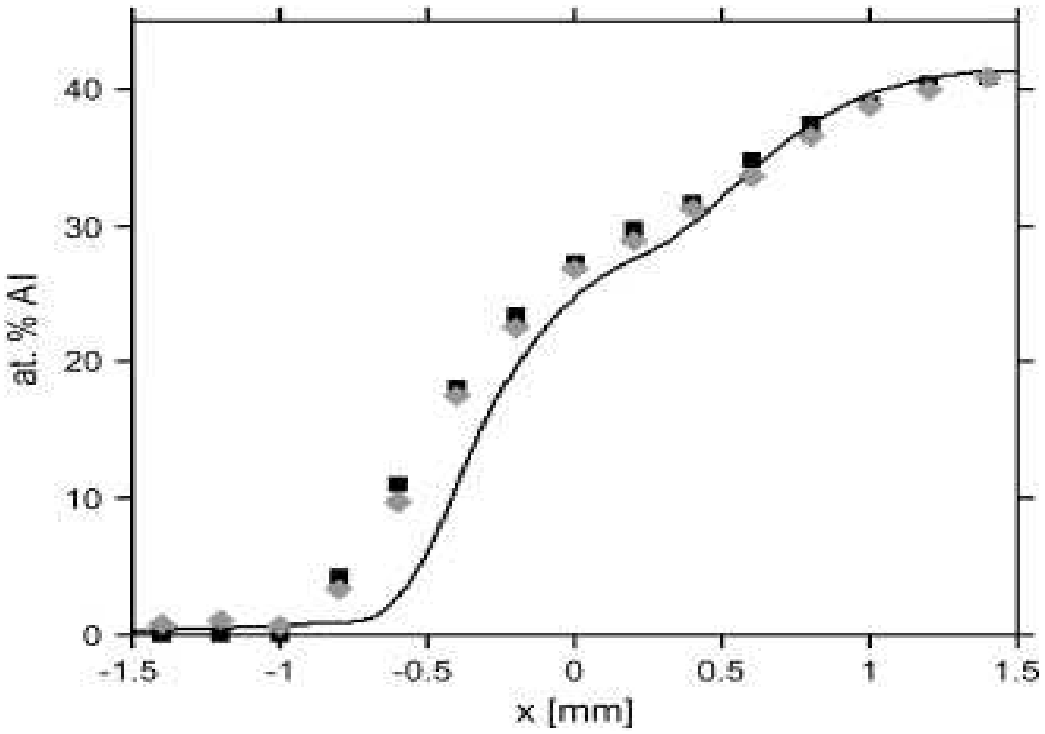

3.3. Oxidation of diffusion couples

Fig. 7a–c shows SEM micrographs of the oxide scale grown on the surface of the diffusion couple prepared with FA alloy. There is a change in the morphology of the scale, as expected, due to the variation in composition. In the absence of aluminium the oxide is composed only of iron oxides; at low aluminium content there is the formation of both iron and aluminium oxides and for high aluminium content the scale is composed only of aluminium oxides. Fig. 7a relates to the region of pure iron where the scale has partially spalled. Under the oxidising conditions used in the present work, the scale should comprise a very thin outermost hematite (Fe_2O_3) layer, a thin intermediate magnetite (Fe_3O_4) layer, and a thick inner wüstite layer (FeO) [19]. At an aluminium content of about 11 at.%, it is observed that the morphology of the oxide becomes more compact (Fig. 7b).

Fig. 7. SEM images of different parts of the iron–FA diffusion couples showing: (i) the surface of the oxide scale (secondary electrons mode) at (a) 0 at.% Al, (b) 11 at.% Al and (c) 41 at.% Al obtained by electrons scattering; and (ii) the thickness of the oxide for (d) 5 at.% Al, (e) 11 at.% Al and (f) 41 at.% Al (back scattering imaging). Before cutting the transverse section, the oxide scale was protected with a Ni layer as indicated in Fig. 7d.

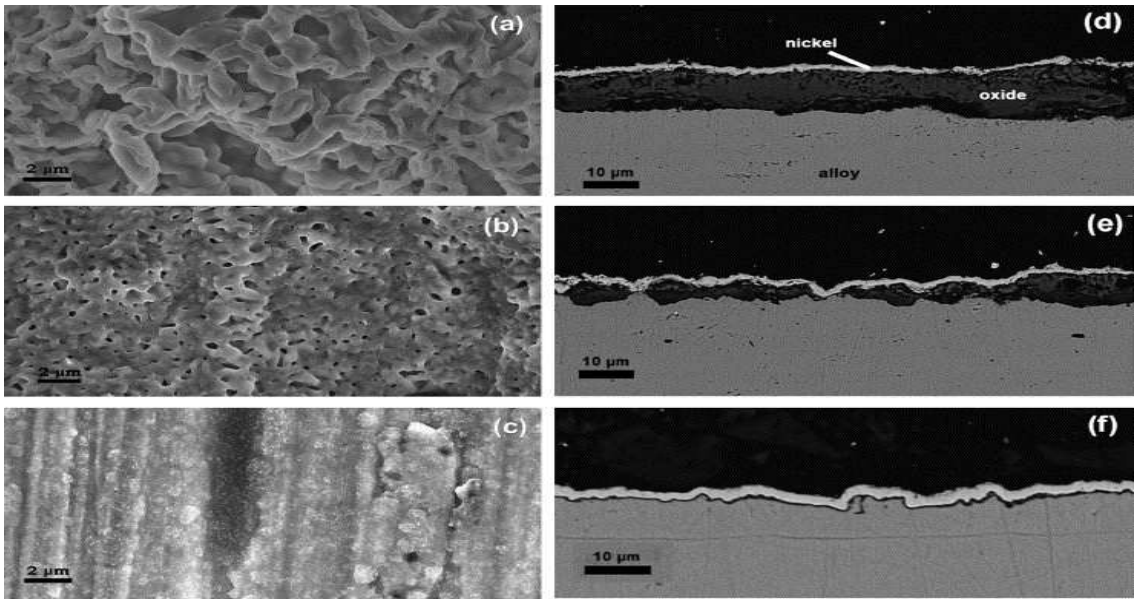

The influence of aluminium content on the scale thickness is illustrated in Fig. 7d–f. An increase in the aluminium content from 5 to 11 at.% leads to a scale half thick. At around 18 at.% Al there is no evidence of any growth of iron oxide nodules any longer. It can thus be assumed that above this aluminium content the scale is composed only of alumina. This result is in agreement with the reported values for suppressing internal oxidation and growth of iron oxides on iron aluminides at temperatures between 800 and 900 °C [20]. The morphology of the scale has been observed to be essentially the same for aluminium contents ranging from 18 to 41 at.%, and there was no evidence of any significant variation in the scale thickness for this range of aluminium contents. The micrographs in Fig. 7c and f are representative for this part of the diffusion couple. Future studies will include the preparation of slices out of these couples to obtain specimens of various compositions within the same phase (A2 and B2) for thermogravimetric test.

4. Conclusions

The relation between chemical composition, microstructure, and oxidation has been studied on four FeAl based alloys. The parabolic oxidation rate, which was measured on thick specimens of the different alloys, showed that the oxide scale consists of alumina. This selective oxidation of aluminium can lead to a significant decrease of the aluminium content

in the alloy, provided the specimen is thin enough. Finally the diffusion couple technique allowed us to prepare specimens with variable composition. The microstructure of such specimens was examined by optical microscopy and SEM, and first results of TEM observation were reported. Further TEM examination is in progress to compare the microstructure of the wedge specimens in the aluminium-depleted zone with those in the diffusion couples, with the aim to look for the possible effect of vacancy injection due to oxidation.

Acknowledgements

This study is related to the COST 535 action “Thalu” and is in part funded by Région Midi-Pyrénées (contract 03007522). One of the authors (MM) acknowledges the Programme Alβan, European Union Programme of High Level Scholarships for Latin America, identification number E03D08330VE.

References

V.S. Rao, V.S. Raja and R.G. Baligidad, *Oxid Met* 57 (2002), p. 449.

C.H. Xu, W. Gao and H. Gong, *Intermetallics* 8 (2000), p. 769.

E. Cadel, D. Lemarchand, A.S. Gay, A. Frackzkiewicz and D. Blavette, *Scripta Mater* 41 (1999), p. 421.

F. Stein, M. Palm and G. Sauthoff, *Intermetallics* 13 (2005), p. 1275.

M.A. Morris, O. George and D.G. Morris, *Mater Sci Eng* A258 (1998), p. 99.

G. Inden and W. Pepperhoff, *Z Metallkd* 81 (1990), p. 770.

Binary alloys phase diagrams (2nd ed.), ASM International (1996) On CD Rom.

M.J. Marcinkowski and N. Brown, *J Appl Phys* 33 (1962), p. 537.

M. Karlík, *Mater Sci Eng* A234–236 (1997), p. 212.

W. Liu, H. Rösner, E. Langmaack, A. Gemperle, J. Gemperlova and J. Pesicka *et al.*, *Mater Sci Eng* A258 (1998), p. 15.

K. Yoshimi, S. Hanada, T. Onuma and M.H. Yoo, *Phil Mag A* 73 (1996), p. 443.

D.G. Morris, L.M. Requejo and M.A. Muñoz-Morris, *Intermetallics* 13 (2005), p. 862.

Colas D. Renforcement d'alliages fer-aluminum B2. Influence d'additions (Ni et B) et de la microstructure. PhD thesis, Ecole Nationale Supérieure des Mines de Saint-Etienne; 2004.

Suzon E. Influence de traitements thermomécaniques, sur les textures, microstructures et propriétés élastiques d'un alliage Fe–40 at. % Al à grains fins. PhD thesis, Université de Metz; 2004.

Martinez M, Viguier B, Maugis P, Lacaze J. In: Microscopy of oxidation, 4–6 April 2005. Birmingham (UK): The University of Birmingham, in press.

W.Y.D. Yuen and R.Y. Chen, *Oxid Met* 59 (2003), p. 433.

M. Salamon, D.H. Fiks and H. Mehrer, *Defect Diffusion Forum* 237–240 (2004), p. 444.

K. Nishida, T. Yamamoto and T. Nagata, *Trans Jpn Inst Met* 12 (1971), p. 310.

N. Birks and G.H. Meier, Introduction to high temperature oxidation of metals, Edward Arnold, London (1983).

P.F. Tortorelli and U.K. Natesan, *Mater Sci Eng* A258 (1998), p. 115.

Corresponding author. Tel.: +33 5 62 88 56 75; fax: +33 5 62 88 56 63.